A Global Climatology of Single-Layer and Overlapped Clouds and Their Optical Properties Developed Using a New Algorithm Applied to Terra/MODIS Data

Fu-Lung Chang [(1)] and Zhanqing Li [(1,2)]

(1) Earth System Science Interdisciplinary Center

(2) Department of Meteorology

University of Maryland, College Park, MD 20742

3 June 2004

Corresponding author: Dr. F.-L. Chang, Earth System Science Interdisciplinary Center, 2207 Computer and Space Sciences Bldg, University of Maryland, College Park, MD 20742.

Email: fchang@essic.umd.edu

Abstract

Knowledge of cloud vertical structure is crucial for climate modeling. Weather satellites have provided reliable information on column-integrated cloud amounts and rough estimates of cloud-top altitude for thick single-layer clouds. Cloud overlapping has been widely recognized by climate modelers, but no reliable information is available yet from any passive satellite sensors. This study develops a near-global climatology of cloud vertical structure and optical properties using a new retrieval method of Chang and Li (2004). Taking full advantage of the multiple channels of the Moderate Resolution Imaging Spectroradiometer (MODIS), the new method can differentiate overlapped cirrus clouds from single-layer water and ice clouds. Based on daytime Terra/MODIS 5-km overcast measurements sampled from January, April, July and October 2001, we deduce the frequency of occurrence, cloud-top pressure/temperature (Pc/Tc), visible optical depth (t_{VIS}), and infrared emissivity (e). Of all overcast scenes, high clouds (Pc < 500 mb) occurred ~52%/61% of the time over ocean/land. Cirrus cloud (e < 0.85) occurred ~35%/41%, of which ~27%/29% (absolute values) were cirrus overlapping water clouds over ocean/ land. Low clouds (Pc > 600 mb) occurred ~71%/65% of the time which include single-layered clouds (~44%/36%) and overlapped clouds (~27%/29%). Between 500-600 mb, there is an extremely low occurrence of Pc (< 4% globally). As such, a distinct bimodal distribution of cloud-top height is found on a global scale with maxima occurring around 275 mb for ice clouds and 725 mb for water clouds. The retrieved cirrus properties show a mean t_{VIS} of ~1.5 and a mean e of ~0.5, which are similar for both overlapped and non-overlapped cirrus clouds. They also agree with the MODIS standard retrievals for single-layer cirrus clouds. Large discrepancies are, however, found with the MODIS emissivity, cloud top height and optical depth products for overlapped clouds for which MODIS does not differentiate the higher and lower clouds.

1. Introduction

Clouds influence the Earth's radiation budget by 1) reflecting solar radiation back to space and 2) trapping longwave radiation in the Earth system. Unlike many low clouds that have more influence on solar radiation through reflection, high cirrus clouds reflect only a small amount of solar radiation, but prevent a large quantity of longwave radiation from leaving the Earth system (Liou 1986). Therefore cirrus clouds usually exert a net radiative heating on the Earth system, rather than cooling as for other cloud types (Ramanathan et al. 1989; Harrison et al. 1990; Hartmann et al. 1992). The horizontal coverage of cirrus clouds and their vertical distribution in the upper atmosphere are also linked to atmospheric circulation and the water cycle (Stephens et al. 1990).

In order to gain a better understanding of the Earth's radiation budget and to improve weather and climate modeling, it is essential to accurately identify these high cirrus clouds and determine their optical properties. Surface observers from land weather stations and ships in the oceans report that multilayer clouds occur ~40% of the time over the Intertropical Convergence Zone (ITCZ) and Southern Pacific Convergence Zone (SPCZ) (Hahn et al. 1982, 1984; Warren et al. 1985). However, they do not provide information on cloud top height/pressure and cloud optical properties and may not be able to identify cirrus clouds when low clouds are present. Indirect observations of cloud vertical structure from global radiosonde water vapor data also indicate that multilayer clouds occur ~40% of the time (Poore et al. 1995; Wang et al. 2000), but their extremely low water vapor in the upper atmosphere can cause large uncertainties in determining cirrus clouds. Active sensors like airborne lidar (Sassen 1991; Platt et al. 1994; Clothiaux et al.

2000) and surface-based radar (Mace and Benson-Troth 2002) can determine more effectively multilayer clouds, but are limited to a few ground locations.

To date, weather satellites are the only tool to measure cloud and climate variables on a global scale, an objective addressed by the International Satellite Cloud Climatology Project (ISCCP) (Rossow and Schiffer 1991; Rossow and Schiffer 1999). However, there is a dearth of information concerning the global climatology of cloud vertical structure and cirrus cloud properties. This is because the often-used visible and infrared measurements made by weather satellites are overwhelmingly affected by thick water clouds. Thin cirrus clouds have so faint signal that are difficult to detect. This makes it problematic to retrieve the optical properties such as optical depth and cloud-top height for either of the overlapped cloud layers. Although high-altitude cirrus clouds are often very thin, their presence can bungle the retrieval of lower thick clouds, leading to large errors in the retrieval of cloud height and optical properties, as demonstrated in this paper and in Chang and Li (2004).

As a result, large uncertainties may exist in the limited cirrus cloud climatologies reported in the past such as the one derived from the ISCCP weather satellite data (1983 to the present) from both geostationary and polar orbiting satellites (Rossow and Schiffer 1991; Jin et al. 1996). In the ISCCP analyses, a bispectral method invoking a visible (~0.6 μm) and an infrared (~11 μm) channel are used in the retrievals of cirrus optical depth and cloud-top height. The bispectral method is used because these two channels are commonly available from all U.S. and international weather satellites (usually ~ 4-8 km at nadir resolution). These data have been proven very useful in depicting the horizontal distribution of clouds on a global scale and the cloud-top heights of optically thick clouds, but they possess little information pertaining to cloud

layering especially for thin cirrus clouds overlapping thick water clouds. This would lead to large uncertainties in cloud vertical structure.

Another cirrus cloud climatology is mainly focused on mid- to high clouds inferred from the multi-year High-resolution Infrared Radiometer Sounder (HIRS) data (~ 17-km nadir resolution) on board the National Oceanic and Atmospheric Administration (NOAA) polar-orbiting satellite (Wylie et al. 1994; Wylie and Menzel 1999). The HIRS analyses used several infrared channels near the 15-μm CO_2 absorbing band in a technique known as the CO_2-slicing method to determine cirrus cloud-top altitude and an effective cirrus cloud amount from the 11-μm channel. They reported that high-level transmissive clouds covered more than 30% of the globe on average and more than 50% at all times in the Tropics. A major uncertainty lies in the large field of view of the HIRS pixel , which increases for oblique angles.

A few experimental techniques have been proposed for applications to Advanced Very High- Resolution Radiometer (AVHRR) data (Baum et al. 1995; Ou et al. 1996) and to Moderate Resolution Imaging Spectroradiometer (MODIS) airborne simulator (MAS) data using 1.6-μm and 11-μm channels (Baum and Spinhirne 2000), but neither has been used for extensive applications. These techniques are primarily concerned with multilayer scene identification and thus do not deal with cloud optical depth retrievals. Other satellite techniques have been proposed for retrieving multilayer clouds over ocean environments using a combination of microwave, visible and infrared imager data (Sheu et al. 1997; Lin et al. 1998; Ho et al. 2003). The large variability of surface emissivity over land limits their applications to over oceans only. Also, only the radiative effective height of a thin cloud can be determined.

The unprecedented MODIS provides imager data at a high spatial resolution (250-m to 1-km nadir resolution, depending on wavelengths) and high spectral resolution at 36 bands (0.415

μm to 14.235 μm) (King et al. 2003). The cloud-top data available from the MODIS standard product provides much better information on cirrus cloud-top height. However, no information is provided concerning if there is any lower cloud beneath the cirrus cloud and thus no appropriation is made to separate the total column-integrated cloud optical depth in terms of high and low clouds. This is because the retrieval assumes a single-layer cloud.

In this study, we applied a new retrieval method developed by Chang and Li (2004) to one year worth of MODIS data for obtaining the climatologies of 1) single-layer water and ice clouds, and two-layer cirrus overlapping water clouds, and 2) the cloud-top altitudes and optical depths of the identified cloud types, and the emissivity of semitransparent clouds. They are retrieved from the MODIS 1-km calibrated visible and infrared radiance data, together with the MODIS cloud mask product (Ackerman et al. 1998), and cloud-top pressure/temperature derived from the CO_2-slicing method (Menzel et al. 2002). We will classify clouds into different categories based on cloud-top pressure (Pc), visible optical depth (t_{VIS}), and 11-μm high-cloud emissivity (e_{hc}), and overlapping information. The frequencies of occurrence and optical properties are analyzed for January, April, July, and October 2001.

Section 2 outlines the MODIS data and the retrieval method. Section 3 describes the overcast scene identification and the determination of the five cloud categories. Section 4 presents the near-global cloud-top vertical structure and the retrieved properties for the overlapped and non-overlapped cirrus clouds, and other high-, mid-, and low-altitude clouds. Section 5 compares the retrieved properties with the current MODIS product and the concluding remarks are given in Section 6.

2. Data and Methodology

a. The MODIS data

The MODIS imager is a central instrument on board two National Aeronautics and Space Administration (NASA) Earth Observing System (EOS) satellites,Terra (launched in December 1999) and Aqua (launched in May 2002). The imager carries 36 onboard calibrated channels/bands (0.415 μm-14.24 μm) (Barnes et al. 1998) and started global observations (in February 2000 for Terra and in June 2002 for Aqua) at high spatial resolutions of 250 m at nadir for two visible channels (bands 1 and 2), 500 m for five near-infrared channels (bands 3-7), and 1 km for bands 8-36. The data used in this study are the 1-km aggregated radiance data (MOD021KM) and the channels used for retrieving cloud optical depth and cloud-top pressure/temperature are one visible (0.65 μm or 0.86 μm) and one infrared (11 μm) channel, similar to those used in generating the standard MODIS cloud products (Platnick et al. 2003). A key additional variable employed is the MODIS CO_2-slicing-derived Pc (and interpreted Tc) (Menzel et al. 2002) for determining the altitude and ambient temperature of the cirrus cloud.

For cloud detection, this study relies on the MODIS Level-2 cloud mask product as processed by the MODIS cloud/clear-sky discrimination algorithm (Ackerman et al. 1998). The MODIS cloud discriminating algorithm is in essence a series of cloud tests applied to as many as 20 of the 36 MODIS channels, depending on surface scene types and solar illumination conditions. While the cloud tests provide much more detailed results, four categories of cloud probability, namely, *confidence clear*, *probably clear*, *probably cloudy*, and *cloudy*, are identified on two spatial resolutions: at 1-km and 5-km (5×5 pixels) scales. In this study, 1-km pixels identified as being probably cloudy or cloudy are classified as overcast with a cloud cover fraction equal to 1. An overcast 5-km scene is identified only if all of the 5×5 1-km pixels are

identified as probably cloudy or cloudy. In this study, cirrus cloud properties are retrieved and analyzed only for the 5-km overcast scenes.

The MODIS Pc and Tc products are currently retrieved on a 5-km (5×5 pixels) basis using two different approaches for low clouds ($Pc \geq 700$ mb) and higher clouds ($Pc < 700$ mb) (Menzel et al. 2002). If a cloud is found to be above 700 mb, Pc is retrieved using the CO_2-slicing method; otherwise, Pc is inferred from the 11-μm brightness temperature. The CO_2-slicing method utilizes four of the MODIS infrared bands within the CO_2 partial absorption regions, i.e., band 33 (13.34 μm), band 34 (13.64 μm), band 35 (13.94 μm) and band 36 (14.24 μm); this choice of bands is known for its effectiveness in detecting thin cirrus clouds. The method has been applied to HIRS data and Geostationary Operational Environmental Satellite (GOES) data as well and demonstrated an accuracy generally within ±50 mb in the retrieved high-cloud Pc. Discussion on the uncertainties of the CO_2-slicing method can also be found in Baum and Wielicki (1994).

For low clouds with $Pc \geq 700$ mb, the CO_2-slicing method loses its sensitivity and effectiveness, therefore MODIS relies on the 11-μm observed radiance to retrieve Tc, instead of Pc. The Tc is also determined on a 5-km scale. Once the Tc of a low cloud is retrieved, a corresponding Pc is inverted using the atmospheric profiles of Pc and Tc derived from the NOAA National Centers for Environmental Prediction (NCEP) Global Data Assimilation System (Derber et al. 1991). A similar Pc-to-Tc inversion is also applied when MODIS uses the CO_2-slicing method for retrieving Pc (< 700 mb), except that Pc is retrieved before Tc is interpreted.

b. The overlapped retrieval algorithm

As mentioned earlier, the MODIS standard products only provide the top of the highest cloud viewable from space, which poses a problem for overlapping clouds. To overcome this limitation, we developed an algorithm that detect the overlapped clouds and retrieve their optical properties. Details of the retrieval algorithm are given in Chang and Li (2004) but a brief discussion is given here. The algorithm first determines the altitude of the high cloud based on the MODIS CO_2-slicing derived Pc. An overlapped or non-overlapped situation is determined only when Pc < 500 mb and $e_{hc} < 0.85$ ($t_{VIS} < \sim 4$) using combined data from the CO_2 slicing channel and 11 μm channel. An automated retrieval procedure determines whether a high-cloud pixel contains single-layered or overlapped high cloud. When an overlapped low cloud is detected, its altitude is inferred from the average cloud-top altitude of the low clouds identified from the neighboring pixels.

For high-cloud ($e_{hc} < 0.85$), the overlapped retrieval begins with a determination of high-cloud infrared optical depth (t_{IR}) following the method of Minnis et al. (1993a) as given by

$$t_{IR} = -m \ln(1 - e_{hc}), \tag{1}$$

where m denotes the cosine of the satellite zenith angle. For an overcast pixel, e_{hc} can be calculated as (e.g., Wylie et al. 1994)

$$e_{hc} = \frac{R(u) - R'(u)}{R_{hc}(u) - R'(u)}, \tag{2}$$

except that

$$R'(u) = e_{lc} R_{lc}(u) + (1 - e_{lc}) R_{clr}(u), \tag{3}$$

where $R(u)$ is the MODIS-observed 11-μm radiance, $R_{hc}(u)$ is the 11-μm equivalent blackbody radiance calculated at the MODIS CO_2-slicing-derived temperature, $R_{clr}(u)$ is the clear-sky 11-μm equivalent blackbody radiance, and e_{lc} and $R_{lc}(u)$ denote the low-cloud 11-μm emissivity and equivalent blackbody radiance, respectively. From Eq.(3), if no low cloud is present, then

$$R'(u) = R_{clr}(u), \tag{4}$$

which is essentially the single-layer model that is used in the MODIS standard retrieval algorithm (Menzel et al. 2002). Note that this has been used for retrievals of both single-layer and overlapped high clouds.

The high-cloud t_{IR} inferred from Eq. (1) can be related to t_{VIS} at visible wavelengths (Minnis et al. 1993a) by

$$t_{VIS} = x t_{IR}. \tag{5}$$

An empirical ratio factor of x = 2.13 is adopted here following the observed mean value from in-situ measurements as derived empirically by Minnis et al. (1990), which is also equal to the theoretical calculations for a cirrostratus hexagonal ice-crystal model (Takano and Liou 1989). The relationship between t_{VIS} and t_{IR} is also used by ISCCP for improving their ice cloud retrieval products (Rossow and Schiffer 1999). It has also been demonstrated that both hexagonal ice-crystal and random fractal poly-crystal models produce similar results in the viewing-scattering angles encountered in satellite observations (Mishchenko et al. 1996).

Equations (1-5) constitute the essential components of our two-layer retrieval algorithm. For the determination of high-cloud t_{VIS}, t_{VIS} for the low cloud is required, and vice-versa. To offset this mutual dependence, single-layer low clouds in neighboring pixels are first sought to

estimate the cloud-top temperature of the lower clouds. If no nearby single-layer cloud is found within the neighborhood of ± 125 km in all directions, no retrieval is performed, but the pixels are included in determining the statistics of overlapping clouds. While we could use the climatological values of low cloud-top temperature as obtained in this study, these cases represent a small fraction of the overlapping clouds (4% in absolute frequency of occurrence, or <10% in relative frequency out of the total overlapped clouds). The retrieval follows an iterative process to determine the best solutions of high-cloud and low-cloud t_{VIS} that generate closest fits to the observed and modeled radiances at both visible and infrared channels.

The retrieval algorithm is implemented through lookup tables in order to accelerate the processing of large volumes of data. They were obtained following extensive radiative transfer simulations in the visible and IR channels for a two-layer cloud system (cirrus above water cloud). The ice-cloud layer adopts a fixed effective radius of r_e =30 μm and uses the scattering phase functions of the fractal ice polycrystals. This follows the ISCCP ice cloud model (Rossow and Schiffer 1999), which has proven to be more favorable based on comparisons with observational data (Minnis et al. 1993b; Francis 1995; Descloitres et al. 1998). In particular, Descloitres et al. (1998) show that the observed angular distributions of the visible reflectances from cirrus clouds agree within a few percent with the calculations based on the fractal-polycrystal scattering phase functions. Liquid water cloud layers have a fixed effective radius of r_e = 10 μm, also following the ISCCP model, and Mie scattering phase functions are used for the water droplets.

Atmospheric transmittance and molecular scattering are calculated in the visible spectrum using the MODTRAN-4 model based on standard U.S. atmospheric temperature and humidity profiles (Berk et al. 1999). The surface albedo data are obtained from the bi-monthly MODIS

Filled Land Surface Albedo Product; for oceanic scenes the surface albedo is assumed to be 0.05. Since the retrieval of high-cloud t_{VIS} primarily relies on the 11-μm e_{hc}, uncertainties in the surface albedo and atmospheric properties have a small effect on its retrieval. But the uncertainties have more influence on the retrieved low-cloud t_{VIS}.

3. Near-global Cloud Properties

a. Overcast scenes and cloud categories

The MODIS data used in this study are from the 5-km overcast scenes observed in January, April, July and October 2001 by the Terra satellite (nominal overpass time 10:30am). It has a near-global coverage and excludes the polar winter regions. The data are sampled every fourth day so that there are eight days (day 2, 6, 10, 14, 18, 22, 26 and 30) sampled from each month. Note that the Terra/MODIS instrument failed between mid-June and July 2 of 2001so the July 4 data was sampled to replace the July 2 data. Use of the sampled data instead of daily data is necessary in order to reduce the data volume and in consideration of sample independence in light of the life cycle of a cloud system. Analyses of these sampled data should provide reasonable global cloud characteristics since synoptic weather systems transit on a time scale of ~ 4–7 days, except for a potential bias due to the diurnal variation of cloud.

Excluded in the processing are surface scene types of ice or snow cover and pixels with a solar zenith angle larger than 75°. It is widely recognized that no reliable retrieval of clouds can be made over bright scenes. The snow/ice surfaces were reported by the National Snow and Ice Data Center's Near real-time Ice and Snow Extent (Armstrong and Brodzik 2001) and are provided in the MODIS 1-km Quality Assurance data (Platnick et al. 2003). These two

constraints eliminated mostly the high-latitude polar region and high-elevation mountainous areas. Also, the near-global coverage data set represents only the daytime observations.

Figure 1 shows an example of the zonal-mean values of total cloud amount (dashed), 5-km overcast amount (solid), and 5-km overcast amount with MODIS Pc < 500 mb (dotted) obtained during April 2001. It is seen that the 5-km overcast amount exhibits a similar latitudinal variation as that of the total cloud amount. The patterns of these latitudinal distributions are similar to previous findings (e.g., Jin et al. 1996), which show more cloud amounts in the Tropics and midlatitudes, but less in subtropical regions. The total near-global cloud amounts for January, April, July and October are similar and around 60% and the total 5-km overcast amounts are also similar and around 45%. These cloud amounts are smaller than the ISCCP cloud amounts (Jin et al. 1996; Rossow and Schiffer 1999). Although the differences may be in part due to the different cloud screening techniques and in part due to different sensors' spatial resolutions, they are beyond the research interests of this study.

From our retrieval scheme, all of the 5-km overcast scenes are classified into five cloud categories (Chang and Li 2004), namely, 1) High1: single-layer high thin clouds (cirrus, Pc < 500 mb and $e_{hc} < 0.85$), 2) High2: high thin cloud overlapped with low clouds (Pc < 500 mb and $e_{hc} < 0.85$), 3) High3: high thick clouds (Pc < 500 mb and $e_{hc} > 0.85$, overlapping is undecided), 4) Low1: low clouds with no cirrus above (Pc > 600 mb, assumed single-layer), and 5) Mid, middle clouds (500 mb ≤ Pc ≤ 600 mb, overlapping is undecided). The overlapped or non-overlapped situations are only determined for Pc < 500 mb, thus all Mid and Low1 clouds are undecided. For high clouds, they are only determined if $e_{hc} < 0.85$, which essentially represents cirrus clouds (Sassen et al. 2002). Thus, High3 are also undecided. The Mid cloud in this study is only an *ad hoc* definition used to separate the high and low clouds. Therefore, some Mid clouds

may be overlapped with cirrus clouds or low clouds, but the percentage of such occurrences should be small as revealed in this study.

Figure 2 shows the latitudinal distributions of the zonal-mean cloud amounts for the five cloud categories. The overall mean values for the five cloud categories are also calculated for each of the four months and are given in Table 1 in terms of the absolute cloud amount (upper rows) and relative percentage out of all 5-km overcast amounts (lower rows). Overall, the two most dominant cloud configurations are single-layer low, and cirrus overlapping with low clouds. The latter accounts for about 30% of all overcast cases, or 50% of all high clouds. It is the most frequently observed multi-layer clouds that occur in nature, according to lidar measurements (D. Winker, private communication). The 30% does not include the 4% of extra overlapping clouds that were not processed due to a lack of single-layer low clouds nearby. So the true frequency is slightly higher. High clouds occurred most frequently over the ITCZ and midlatitudes and are seldom in the subtropics. Tropical high clouds are associated with extensive anvil cirrus clouds covering large spatial domains. In higher latitudes, they are accompanied by storms and fronts, as revealed from ground observations (e.g., Warren et al. 1985). The optically thick high clouds (High3) with $e_{hc} > 0.85$ are also more frequent in the Tropics due to deep convection and over midlatitudes due to mesoscale cyclones. Even though their absolute cloud amounts are similar, relatively more high clouds are found over land than over ocean.

There are fewer low clouds (Low1) than total high clouds (High1+High2+High3), especially over land. This is partially because the satellite views from above so that high clouds may obscure lower clouds. So in regions of prevailing high clouds, low clouds would be missed which we attempt to “recover” for the frequently-occurring cirrus over water clouds.

b. A bimodal distribution of cloud vertical structure

Figure 3 shows the monthly frequency distributions of Pc. To better visually display the vertical structure of all clouds, the curves representing different categories are recombined. For example, the same curve is used for single-layer low, mid-level and high clouds because their altitudes are indicated by Pc itself. On the other hand, an overlapped low cloud (Low2) is added that has the same total frequency of occurrence as High2. Of course, Low2 and High2 are from the same overlapped clouds but they differentiate the higher and lower portions. The total frequencies of all cloud types are also plotted.

From the figure, a distinct bimodal Pc distribution is seen, with a universal minimum at around 530 mb in each sub-panel and two maxima at around 275 mb and around 725 mb. When including all MODIS-retrieved Pc, i.e. not limited to the 5-km overcast pixels, we found less than 4% of clouds having their tops falling between 500 mb and 600 mb. The bimodal Pc distribution corresponds to two typical cloud systems: 1) dominant low-level stratiform clouds, like shallow cumulus and stratocumulus, which are often organized into cloud bands and patches (Kuettner 1971; Agee 1984); and 2) high clouds resulting from synoptic weather systems, like midlatitude fronts and cyclones and tropical storms, which are often organized into large-scale patterns of cirrus clouds, squall lines, and deep convective clouds (Starr and Cox 1985; Sheu et al. 1997). Note that the two-layer pattern is not a direct consequence of using the two-layer retrieval algorithm, as a cloud top may be located anywhere. It is true, however, that the algorithm cannot retrieve more than two layers of cloud and thus the retrieved low clouds may represent the average of all multilayer low clouds beneath the cirrus as identified from the neighboring pixels. There is no hope to resolve multi-layer low clouds, unless ground-based or space-borne radar are used (Mace et al. 2001; Stephens et al. 2002). Fortunately, high thin cirrus

over water clouds occur much more frequently than multi-layer low clouds (Winker, private communication).

The occurrence of a minimum Pc as shown in the figure is similar to the finding of minimum cloudiness from previous sounding data obtained during the Tropical Ocean Global Atmosphere Coupled Ocean-Atmosphere Response Experiment (TOGA COARE) (Zuidema, 1998). However, in other studies concerning the distribution of tropical convection (Liu and Moncrieff 1998; Johnson et al. 1999), a trimodal characteristic of tropical cumulus cloud types is suggested that exits over the Pacific warm pool and the tropical eastern Atlantic. They are characterized as shallow cumulus (tops near 2 km), deep cumulonimbus (tops near tropopause), and cumulus congestus (tops between 4.5 and 9.5 km) and the three cloud populations can vary significantly with seasons. It is noted that our overlapped scheme cannot retrieve any multi-layer situation for such deep cumulonimbus and cumulus congestus clouds. Nonetheless, on a global scale, there exists a predominant bimodal Pc distribution. An understanding of this ubiquitous vertical structure is crucial, as cloud vertical distribution influences the radiative and latent heating profiles of the atmosphere, which in turn influences both small-scale and large-scale dynamics and the atmospheric general circulation (Ramaswamy and Ramanathan 1989; Randall et al. 1989; Sherwood et al. 1994). More verification of the cloud vertical structure is required.

Figure 4 shows the monthly frequency distribution of t_{VIS} for the six cloud categories and in total. The t_{VIS} intervals are plotted following the ISCCP (Rossow and Schiffer 1999) , i.e. 0-1.3, 1.3-2.2, 2.2-3.6, 3.6-5.8, 5.8-9.4, 9.4-14.8, 14.8-23, 23-36, 36-60, and >60. The mean Pc, Tc, and t_{VIS} calculated from each month are given in Table 2 for each cloud category as shown in Figs. 3 and 4. Clearly, cirrus clouds single-layer (High1) or overlapped (High2), have the smallest t_{VIS} (< 4) among all cloud types, as expected. A large number of cirrus t_{VIS} peak at ~1.0,

which is dominated by cirrus clouds overlapping low clouds. The low clouds seem to form another peak at t_{VIS} ~8, but the distribution is much broader with a skewed mean of t_{VIS} ~ 11 for Low1 and ~13 for Low2.

The overall frequencies of occurrence of the 5-km overcast Pc and t_{VIS} from the four-month near-global dataset over ocean and land are shown in Fig. 5. The upper panels represent the MODIS standard product that applies the single-layer cloud retrieval model and the lower panels are from the overlapped retrievals. Both the Pc and t_{VIS} intervals follow the ISCCP (Rossow and Schiffer 1991), where Pc intervals are at 1000-900 mb, 900-800 mb, 800-740 mb, 740-680 mb, 680-620 mb, 620-560 mb, 560-500 mb, 500-440 mb, 440-375 mb, 375-310 mb, 310-225 mb, 225-180 mb, 180-115 mb, and 115-50 mb. The numbers in each panel indicate the total cloud amounts obtained over ocean (left sub-panel) and over land (right sub-panel) and are given separately for Pc < 530 mb and Pc ≥ 530 mb. It should be emphasized that the MODIS only provides the height of the very top layer of a cloud. Through our retrieval, ~12% (absolute frequency of occurrence or about 27% and 29% relative values) of the clouds of high tops were determined to contain low clouds that overlap with high cirrus clouds. If one uses the MODIS cloud top data alone to determine the fractions of high and low clouds, the latter would be substantially underestimated.

Likewise, the MODIS t_{VIS} retrievals do not differentiate high and low clouds, except for providing a single cloud top height. Apparently, attributing the retrieved t_{VIS} to the cloud as designated by the MODIS cloud top would significantly overestimate t_{VIS} for true high-clouds whose optical depths should be much less than lower water clouds. The values of t_{VIS} for the high clouds as seen in Fig. 5a are actually the sum of both high and low clouds. This is

confirmed with a preliminary comparison against the Atmospheric Radiation Measurement (ARM) ground-based radar observations of cloud vertical structure (Chang and Li 2004). Another bias arises in choosing a cloud model for retrieving t_{VIS} for the two-layered ice-over-water clouds. Regarding such overlapped clouds as single-layer clouds, use of either a water or ice cloud model can lead to significant biases.

c. Latitudinal distributions of Pc, Tc, and t_{VIS}

Figure 6 shows the variations of zonal-mean Pc (Fig. 6a), Tc (Fig. 6b), and t_{VIS} (Fig. 6c) corresponding to each of the six cloud categories. From Fig. 6a, Pc for the High1, High2, and High3 clouds changes the most between 200–400 mb; it is highest (~200 mb) in the Tropics and lowers toward higher latitudes. Pc for Low1 and Low2 clouds varies mostly between 680–800 mb with a much weaker latitudinal variability. From Fig. 6b, the high clouds are found mostly between 215–245 K with the lowest Tc in the Tropics (~ 215K). For the low-clouds which have similar Pc, their Tc decreases from ~285 K in the Tropics to less than 270 K at higher latitudes, a trend similar to surface temperature. Differences in Tc (Pc) between the high clouds and the low clouds are thus largest in the Tropics and smallest at higher latitudes. Some dips in the Pc and Tc around 15°-30° in both hemispheres are attributed to the subtropical subsidence regions. The Mid cloud Pc and Tc are also plotted in the figures for reference.

Although similar latitudinal distributions are seen among High1, High2, and High3 clouds and between Low1 and Low2 clouds, the Pc and Tc of High2 clouds are systematically larger (lower in altitude) than those of High1 and High3 clouds. Likewise, the Pc and Tc of Low2 clouds are systematically smaller (higher in altitude) than those of Low1 clouds. The

former is attributed to errors in the single-layer cloud assumption as adopted in the MODIS CO_2-slicing retrieval algorithm where the influence of the underlying low-cloud effect was not taken into account. Menzel et al. (2002) suggest that such errors caused by the presence of underlying low clouds should be smaller than 100 mb. Our results here show a mean bias (High2 minus High1) of about 40 mb in Pc and about 7 K in Tc (cf. Table 2).

As for the differences between Low1 and Low2 clouds, the Pc (Tc) of Low2 clouds is on average smaller by about 50 mb (~2 K) than the Pc (Tc) of Low1 clouds. This difference is likely due to the following two reasons: 1) Since low-cloud Tc is determined first using 11-μm radiance and since Low2 clouds are identified with the presence of High2 clouds, the 11-μm radiance of Low2 clouds can be contaminated by high clouds and result in a smaller Tc and Pc; 2) all Low2 clouds are inferred from part of the Low1 clouds near high-cloud active regions, but Low1 clouds also include extensive areas with low clouds only. So, dynamically the Low2 cloud tops may have developed higher in the atmosphere than those of Low1 clouds, resulting in a smaller Low2 Tc. Unfortunately, we cannot verify in this study if this is really the case.

In comparisons of t_{VIS} (Fig. 6c), High1 and High2 clouds have the smallest t_{VIS} (1.3–1.7), which is expected for thin cirrus clouds with $e_{hc} < 0.85$. There is little difference in the mean t_{VIS} between High1 and High2 clouds, despite the latter being slightly larger than the former. Another notable feature is that in July (cf. Table 2) both High1 and High2 cirrus clouds have the largest t_{VIS} among the four months; however, their total frequencies of occurrence are the least among the four months (cf. Table 1). This is similar to the finding based on the ground-based observations at Southern Great Plains using active remote sensors (Gerald Mac*e*, personal communications). Among all cloud categories, High3 clouds have the largest t_{VIS} on average

(~22 over ocean and ~21 over land) and Mid clouds have the second largest t_{VIS} (~17 over ocean and ~15 over land); Low1/Low2 clouds, on average, have smaller t_{VIS} (~10–14). These differences may be due to cloud geometrical vertical extent. Also, t_{VIS} for Low2 clouds is larger than for Low1 clouds, which may be due to cirrus contamination as mentioned earlier, or may be due to the possibility that the low clouds near the cirrus-overlapped area are thicker than those far away from the cirrus clouds.

The near-global distributions of cloud amount obtained for January, April, July and October 2001 are shown in Figure 7 for all high clouds (High1, High2 and High3), in Figure 8 for overlapped cloud amount (High2/Low2), in Figure 9 for the Mid cloud, and in Figure 10 for the total low clouds (Low1 plus the overlapped Low2). In general, high clouds and overlapped cirrus clouds are widespread, frequently covering the ITCZ, the tropical warm pool (from the western Pacific to the Indian Ocean), and midlatitude storm tracks in both northern and southern hemispheres. It also appears that there are more high clouds in January and April and less in July. There are very few Mid clouds and these tend to be scattered in different places but are mostly located in high latitudes during the summer. On the contrary, low clouds are found everywhere in all seasons with cloud amounts much higher in the midlatitudes (30-60 degrees).

4. Comparisons with the MODIS standard products

In our retrievals, t_{VIS} for cirrus clouds , single-layered (High1) and overlapped (High2), was estimated through an infrared radiative transfer scheme. It is unlike the standard MODIS retrieval algorithm that uses reflectance measurements for cirrus retrieval, which has more bearing on the uncertainty of the ice-crystal scattering phase functions. Figure 11 shows an

example of the latitudinal distributions of t_{VIS} obtained from the MODIS standard product for the cloud categories of High1, High2, High3, Mid and Low1. The figure shows April only, but the patterns of January, July, and October are similar. The monthly-mean MODIS t_{VIS} obtained for the five cloud categories are given in Table 3. In comparison to the same case but obtained from our algorithm as is shown in Fig. 6c, the latitudinal distributions of t_{VIS} are very similar, except for the large differences for overlapped clouds that were separated by our algorithm, but not by the MODIS.

Figure 12 compares the zonal-mean High1 t_{VIS} derived from our infrared method and from the MODIS visible channels of a) 0.86-μm for over ocean and b) 0.65-μm for over land. It is seen that the visible-retrieved cirrus t_{VIS} are on average larger by ~0.25 (a bit more over land) than the infrared-retrieved t_{VIS}, which may be due to various uncertainties like surface reflectance, choice of ice-crystal scattering phase function, infrared-visible t conversion, and ice-particle size, etc. Note that MODIS also retrieves an ice-crystal r_e together with the cirrus t_{VIS}, whereas r_e is not a variable in the infrared retrieval. The relationship given by Eq. (4), used for converting t_{IR} to t_{VIS}, may also be uncertain. The biased slope of the linear regressions may imply that the ratio factor $x = 2.13$ is underestimated. To get results in agreement with the MODIS product, we could change the ratio factor to $x = 2.52$ for over ocean and $x = 2.56$ for over land, but we cannot be sure if this would be physically sound.

The MODIS High3 t_{VIS} as shown in Table 3 are also significantly larger than our retrievals shown in Table 2. This may be because all High3 clouds were assumed to be ice clouds in this study but part of these High3 clouds were retrieved as water clouds by MODIS. The water-cloud model usually leads to a larger t_{VIS} retrieval than the ice-cloud model (Chang and Li

2004) due to the different scattering phase functions of water droplets and ice crystals. Other than for high clouds, the t_{VIS} from MODIS and this study agree well in both Mid and Low1 categories.

Figure 13 shows the latitudinal distributions of zonal-mean e_{hc} (April only) obtained for the High1, High2, and High3 cloud categories. The High1 and High3 e_{hc} from our retrievals are the same as from the MODIS standard products. However, High2 e_{hc} (lines with open points) are from our retrievals whereas High2* e_{hc} (lines with solid points) are from the MODIS products. These two different e_{hc} were both calculated using Eq. (2) except that the calculations of High2* assume that $R'(u) = R_{clr}(u)$ without accounting for the low-cloud effect. The corresponding global mean e_{hc} for all the months are given in Table 2 for High1, High2, and High3 clouds and in Table 3 for High2* clouds. As seen from the figure and tables, the single-layer cirrus (High1) and the overlapped cirrus (High2) both have similar mean e_{hc} with differences less than ±0.01-0.02. However, if no correction is made to account for the overlapping effect, as in the case of High2*, the mean e_{hc} can be significantly overestimated by a magnitude of ~0.10. This difference in e_{hc} (20% relative) leads to an overestimate in t_{VIS} of ~ 0.5, or 30% of the mean t_{VIS}.

Since the MODIS CO_2-slicing technique assumes a single-layer cloud, the MODIS-retrieved Pc for the overlapped High2 clouds is also biased. On a first-order approximation to correct for the MODIS Pc biases in overlapped cirrus clouds, we propose an empirical formula, which is given by

$$\frac{\Delta \mathrm{Pc}}{\Delta e_{hc}} = \frac{(\mathrm{Pc} - \mathrm{Pc}^*)}{(e_{hc} - e_{hc}^*)} \qquad (6)$$

where Pc* and e_{hc}* denote the biased values from the MODIS products, e_{hc} denotes the value from our retrieval, and ΔPc and Δe_{hc} denote the mean biases. The corrected Pc is thus given by

$$\mathrm{Pc} = \mathrm{Pc}^* + \frac{\Delta \mathrm{Pc}}{\Delta e_{hc}}(e_{hc} - e_{hc}^*). \qquad (7)$$

The mean biases can be estimated from the data obtained in this study, for example, ΔPc = 38 mb for over ocean (36 mb for over land) as estimated by High2 minus High1 (Table 2) and Δe_{hc} = 0.11 (0.10) for over ocean (land) as determined by High2* (Table 3) minus High1 (Table 2). The formula can also be applied to correct cirrus-cloud Tc. Note that the calculations of e_{hc} would also depend on the modified cirrus Tc, but fortunately the calculated e_{hc} is much less sensitive to biases in cirrus Tc as compared to biases in low-cloud Tc. For the data analysis presented in this study, we do not modify the MODIS CO_2-slicing-derived Tc (or Pc). However, decreasing cirrus Tc by 6–7 K will decrease the mean e_{hc} by about 0.01-0.02, which are still within the uncertainties of the differences between High1 and High2 e_{hc} (Table 2).

5. Concluding Remarks

The global distribution of cloud vertical structure is crucial to climate studies due to its impact on both the magnitude and sign of net cloud radiative forcing and the adiabatic heating profile of the atmosphere. So far, we have a very poor knowledge of cloud vertical distribution on a global scale, due to the limited channel information (essentially one visible and one infrared)

that may provide bulk information for single-layer clouds, but cannot resolve the vertical distribution in any detail, especially for semi-transparent cirrus overlapping low clouds.

The significantly advanced MODIS instrument provides much richer information, but the current standard MODIS cloud products employ a single-layer cloud model that cannot separate high and low overlapped clouds. To overcome these limitations, a new method was developed that can differentiate single-layer and overlapped clouds and retrieve their individual optical properties (Chang and Li 2004). The new method was applied to near-global MODIS data acquired in January, April, July and October of 2001. The data were sampled one out of every four days. Calibrated radiance data from the 1-km resolution aggregated cloud product (MOD021KM) were processed. The analyses are limited to 5-km overcast scenes due to the coarser resolution of the CO_2 slicing data. They represent approximately 75% of the total global cloud coverage which has a global cloud cover fraction of about 0.60 excluding polar winter regions. We classified clouds into six categories: single-layer high, low and mid-level clouds, overlapped high and low clouds, and thick high clouds. Their frequency of occurrence, cloud-top pressure/temperature, optical depth, and high-cloud emissivity are derived.

Of all 5-km overcast scenes that are processed in this study, the following temporal frequencies of occurrence were obtained. The results are separated over ocean and land with the frequencies over land are given in parentheses: 52% (61%) for high clouds with Pc < 500 mb, ~35% (~41%) for high cirrus clouds with $e_{hc} < 0.85$, 27% (~29%) for high cirrus clouds overlapped with low clouds,, ~71% (65) for low clouds having Pc > 600 mb, in which ~44% (36%) for single-layer low clouds. The remaining middle clouds with a cloud top altitude between 500–600 mb occurred less than 4% over both ocean and land. The retrieved cirrus

clouds have a mean value of t_{VIS} ~1.5 and e_{hc} ~0.5, which are very similar for both the single-layer and overlapped cirrus clouds.

The majority of cloud-top heights occur in two distinct layers, one in the upper troposphere and one in the lower troposphere. The former has a maximum at around 275 mb and the latter has a maximum at around 725 mb. It is a ubiquitous phenomenon occurring at almost all latitudes and in all seasons. In between is a distinct region of extremely low occurrence (< 4%) of cloud tops between 500 mb and 600 mb. This characteristic may shed light on understanding cloud dynamical and radiative processes for improving cloud and climate modeling. Note that these results do not result from the use of our two-layer retrieval model, as the model can identify and retrieve both single and two-layers clouds at any altitude. However, multi-layer clouds below thick high clouds could be missed by this and any other method.

As the MODIS products only provide one cloud top for both single-layer and overlapped clouds, use of these cloud top data would underestimate the low clouds by 30% that overlap with high cirrus clouds whose optical depths would be overestimated by a factor of about 7. In comparison with the ISCCP global cloud climatology presented in Zhang et al. (2004), there also exist large discrepancies. ISCCP has much more middle cloud and less high and low clouds therefore ISCCP does not show a distinct two-layer cloud structure. More detailed comparisons will be conducted and presented in the future.

In light of such substantial differences in the cloud vertical structure that result simply from different inversion algorithms, much caution is warranted in validating general circulation models (GCMs) and improving their cloud parameterization schemes. At present, results of cloud simulations from many GCMs have been validated against ISCCP total cloud amounts, promoting many improvements in the models. Increasing attention is now being paid to more

detailed comparisons that concern the vertical distribution of clouds. For example, the current ARM Cloud Parameterization and Modeling (ARMCPM) working group have collected and analyzed 10 sets of GCM-simulated cloud layer data and compared them to the statistics of the ISCCP (Zhang et al. 2004). It was found that most GCMs produce substantially less middle and low clouds than the ISCCP. In general, compared to that of the ISCCP, the GCMs' mid-level cloud amounts are closer to our new retrieval products, whereas the GCMs' low cloud amounts are even further away from our retrievals. Clearly, it is very critical to sort out these differences in order to improve the performance of GCMs and other types of models of better resolution.

Acknowledgements

This research would not have been possible without the dedicated work of the MODIS Atmospheres Team in processing the cloud mask and cloud properties. The authors are grateful to the NASA Goddard Earth Sciences (GES) Distributed Active Archived Center (DAAC) for providing the MODIS data. Funding for this work was supported by the DOE grant DE-FG02-01ER63166 under the ARM program and NASA grant NNG04GE79G.

References

Ackerman, S. A., K. I. Strabala, W. P. Menzel, R. A. Frey, C. C. Moeller, and L. E. Gumley, 1998: Discriminating clear-sky from clouds with MODIS, *J. Geophys. Res.*, **103**, 32,141-32,158.

Agee, E. M., 1984: Observations from space and thermal convection: A historical perspective, *Bull. Amer. Meteor. Soc.*, **65**, 938-949.

Armstrong, R. L., and M. J. Brodzik, 2001: Recent northern hemisphere snow extent: A comparison of data derived from visible and microwave satellite sensors, *Geophys. Res. Lett.*, **28**, 3673-3676.

Barnes, W.L., T.S. Pagano, and V.V. Salomonson, 1998: Prelaunch characteristics of the Moderate Resolution Imaging Spectroradiometer (MODIS) on EOS-AM1, *IEEE Trans. Geosci. Remote Sens.*, **36**, 1088-1100.

Baum, B. A., and B. A. Wielicki, 1994: Cirrus cloud retrieval using infrared sounding data: Multilevel cloud errors, *J. Appl. Meteor.*, **33**, 107-117.

Baum, B. A., T. Uttal, M. Poellot, T. P. Ackerman, J. M. Alvarez, J. Intrieri, D. O'C. Starr, J. Titlow, V. Tovinkere, and E. Clothiaux, 1995: Satellite remote sensing of multiple cloud layers, *J. Atmos. Sci.*, **52**, 4210-4230.

Baum, B. A., and J. D. Spinhirne, 2000: Remote Sensing of cloud properties using MODIS airborne simulator imagery during SUCCESS. 3. Cloud Overlap, *J. Geophys. Res.*, **105**, 11,793-11,804.

Berk, A., and Coauthors, 1999: MODTRAN4 v. 2.0 User's Manual. Air Force Geophysics Laboratory Tech. Rep. AFGL-TR-89-0122. 98 pp. Available from Air Force Mat. Comm., Hanscomb AFB, Mass..

Chang, F.-L., and Z. Li, 2004: Detecting cirrus-overlapping-water clouds and retrieving their optical properties using MODIS data, submitted.

Clothiaux, E. E., T. P. Ackerman, G. G. Mace, K. P. Moran, R. T. Marchand, M. Miller, and B. E. Martner, 2000: Objective determination of cloud heights and radar reflectivities using a combination of active remote sensors at the ARM CART Sites, *J. Appl. Meteor.*, **39**, 645–665.

Derber, J. C., D. F. Parrish, and S. J. Lord, 1991: The new global operational analysis system at the National Meteorological Center, *Weather Forecasting*, **6**, 538-547.

Descloitres, J. C., J. C. Buriez, F. Parol, and Y. Fouquart, 1998: POLDER observations of cloud bidirectional reflectances compared to a plane-parallel model using the International Satellite Cloud Climatology Project cloud phase functions, *J. Geophys. Res.*, **103**, 11,411-11,418.

Francis, P. N., 1995: Some aircraft observations of the scattering properties of ice crystals, *J. Atmos. Sci.*, **52**, 1142-1154.

Hahn, C. J., and Coauthors, 1982: Atlas of simultaneous occurrence of different cloud types over the ocean. NCAR tech. Note, TN241 + STR, 209 pp. Available from National Center for Atmospheric Research, Boulder, CO 80307.

Hahn, C. J., S. G. Warren, J. London, R. M. Chervin, and R. Jenne, 1984: Atlas of simultaneous occurrence of different cloud types over land. NCAR Tech. Note TN-241 + STR, 216 pp. Available from National Center for Atmospheric Research, Boulder, CO 80307.

Harrison, E. F., P. Minnis, B. R. Barkstrom, V. Ramanathan, R. D. Cess, and G. G. Gibson, 1990: Seasonal variation of cloud radiative forcing derived from the earth radiation budget experiment, *J. Geophys. Res.*, **95**, 18,687-18,703.

Hartmann, D. L., M. E. Ockert-Bell, and M. L. Michelsen, 1992: The effect of cloud type on the Earth's energy balance Global analysis, *J. Climate*, **5**, 1281-1304.

Ho, S.-P., B. Lin, P. Minnis, T.-F. Fan, 2003: Estimates of cloud vertical structure and water amount over tropical oceans using VIRS and TMI data, *J. Geophys. Res.*, **108**, AAC 10 1-16.

Jin, Y., W. B. Rossow, and D. P. Wylie, 1996: Comparison of the climatologies of high-level clouds from HIRS and ISCCP, *J. Climate*, **9**, 2850-2879.

Johnson, R. H., T. M. Rickenbach, S. A. Rutledge, P. E. Ciesielski, and W. H. Schubert, 1999: Trimodal characteristics of tropical convection. *J. Climate*, **12**, 2397-2418.

King, M. D., W. P. Menzel, Y. J. Kaufman, D. Tanre, B. C. Gao, S. Platnick, S. A. Ackerman, L. A. Remer, R. Pincus, and P. A. Hubanks, 2003: Cloud and aerosol properties, precipitable water, and profiles of temperature and humidity from MODIS, *IEEE Trans. Geosci. Remote Sens.*, **41**, 442-458.

Kuettner, J. P., 1971: Cloud bands in the earth's atmosphere, *Tellus*, **23**, 404-425.

Liou, K. N., 1986: Influence of cirrus clouds on weather and climate processes: A global perspective, *Mon. Wea. Rev.*, **114**, 1167-1199.

Lin, B., P. Minnis, B. Wielicki, D. R. Doelling, R. Palikonda, D. F. Young, and T. Uttal, 1998: Estimation of water cloud properties from satellite microwave, infrared and visible measurements in oceanic environment: 2. Results, *J. Geophys. Res.*, **103**, 3887-3905.

Liu, C., and M. W. Moncrieff, 1998: A numerical study of the diurnal cycle of tropical oceanic convection. *J. Atmos. Sci.*, **55**, 2329-2344.

Mace, G. G., E. E. Clothiaux, T. A. Ackerman, 2001: The composite characteristics of cirrus clouds: Bulk properties revealed by one year of continuous cloud radar data, *J. Climate*, 1**4**, 2185-2203.

Mace, G. G., and S. Benson-Troth, 2002: Cloud-layer overlap characteristics derived from long-term cloud radar data, *J. Climate*, 1**5**, 2505-2515.

Menzel, W. P., B. A. Baum, K. I. Strabala, and R. A. Frey, 2002: Cloud top properties and cloud phase-Algorithm Theoretical Basis Document: ATBD-MOD-04, 61 pp. Available at http://modis-atmos.gsfc.nasa.gov/_docs/atbd_mod04.pdf.

Minnis, P., D. F. Young, K. Sassen, J. M. Alvarez, and C. J. Grund, 1990: The 27-28 October 1986 FIRE IFO Cirrus Case Study: Cirrus parameter relationships derived from satellite and lidar data, *Mon. Wea. Rev.*, **118**, 2402-2425.

Minnis, P., K.-N. Liou, and Y. Takano, 1993a: Inference of cirrus cloud properties using satellite-observed visible and infrared radiances. Part I: Parameterization of radiance field, *J. Atmos. Sci.*, **50**, 1279-1304.

Minnis, P., P. W. Heck, and D. F. Young, 1993b: Inference of cirrus cloud properties using satellite-observed visible and infrared radiances. Part II: Verification of theoretical cirrus radiative properties, *J. Atmos. Sci.*, **50**, 1305-1322.

Mishchenko, M. L., W. B. Rossow, A. Macke, and A. A. Lacis, 1996: Sensitivity of cirrus cloud albedo, bidirectional reflectance, and optical thickness retrieval accuracy to ice-particle shape, *J. Geophys. Res.*, **101**, 16,973-16,985.

Ou, S. C., K. N. Liou, and B. A. Baum, 1996: Detection of multilayer cirrus cloud systems using AVHRR data: Verification based on FIRE-II IFO composite measurements, *J. Appl. Meteorol.*, **35**, 178-191.

Platnick, S., M. D. King, S. A. Ackerman, W. P. Menzel, B. A. Baum, J. C. Riedi, and R. A. Frey, 2003: The MODIS cloud products: Algorithms and examples from Terra, *IEEE Trans. Geosci. Remote Sens.*, **41**, 459-473.

Platt, C. M. R., and coauthors, 1994: The Experimental Cloud Lidar Pilot Study (ECLIPS) for cloud-radiation research, *Bull. Amer. Meteor. Soc.*, **75**, 1635-1654.

Poore, K., J. Wang, and W. B. Rossow, 1995: Cloud layer thicknesses from a combination of surface and upper-air observations, *J. Climate*, **8**, 550-568.

Ramanathan, V., R. D. Cess, E. F. Harrison, P. Minnis, B. R. Barkstrom, E. Ahmad, and D. L. Hartmann, 1989: Cloud radiative forcing and climate: Results from the Earth Radiation Budget Experiment, *Science*, **243**, 57-63.

Ramaswamy, V., and V. Ramanathan, 1989: Solar absorption by cirrus clouds and the maintenance of the tropical upper troposphere thermal structure, *J. Atmos. Sci.*, **46**, 2293-2310.

Randall, D. A., Harshvardhan, D. A. Dazlich, and T. G. Gorsetti, 1989: Interactions among radiation, convection, and large-scale dynamics in a general circulation model, *J. Atmos. Sci.*, **46**, 1944-1970.

Rossow, W. B., and R. A. Schiffer, 1991: ISCCP cloud data products, *Bull. Amer. Meteor. Soc.*, **72**, 2-20.

Rossow, W. B., and R. A. Schiffer, 1999: Advances in understanding clouds from ISCCP, *Bull. Amer. Meteor. Soc.*, **80**, 2261-2287.

Sassen, K., 1991: The polarization lidar technique for cloud research: A review and current assessment, *Bull. Amer. Meteor. Soc.*, **72**, 1848-1866.

Sassen, K., Z. Wang, C. M. R. Platt, J. M. Comstock, 2002: Parameterization of infrared absorption in midlatitude cirrus clouds, *J. Atmos. Sci.*, 60, 428–433.

Sherwood, S. C., V. Ramanathan, T. P. Barnett, M. K. Tyree, and E. Roeckner, 1994: Response of an atmospheric general circulation model to radiative forcing of tropical clouds, *J. Geophys. Res.*, **99**, 20,829-20,845.

Sheu, R.-S., J. A. Curry, and G. Liu, 1997: Vertical stratification of tropical cloud properties as determined from satellite, *J. Geophys. Res.*, **102**, 4231-4245.

Starr, D. O'C., and S. K. Cox, 1985: Cirrus clouds. Part II: Numerical experiments on the formation and maintenance of cirrus, *J. Atmos. Sci.*, **42**, 2682-2694.

Stephens, G. L., and coauthors, 2002: The CLOUDSAT mission and the A-Train, *Bull. Amer. Meteor. Soc.*, **83**, 1771-1790.

Stephens, G. L., S.-C. Tsay, P. W. Stackhouse, Jr., and P. J. Flatau, 1990: The relevance of the microphysical and radiative properties of cirrus clouds to climate and climate feedbacks, *J. Atmos. Sci.*, **47**, 1742-1753.

Takano, Y., and K.-N. Liou, 1989: Solar radiative transfer in cirrus clouds. Part I: Single scattering and optical properties of hexagonal ice crystal, *J. Atmos. Sci.*, **46**, 3-19.

Wang, J., W. B. Rossow, and Y. Zhang, 2000: Cloud vertical structure and its variations from a 20-yr global rawinsonde data set, *J. Climate*, **13**, 3034-3056.

Warren, S. G., C. J. Hahn, and J. London, 1985: Simultaneous occurrence of different cloud types, *J. Climate Appl. Meteor.*, **24**, 658-667.

Wylie, D. P., W. P. Menzel, H. M. Woolf, and K. I. Strabala, 1994: Four years of global cirrus cloud statistics using HIRS, *J. Climate*, **7**, 1972-1986.

Wylie, D. P., and W. P. Menzel, 1999: Eight years of high cloud statistics using HIRS, *J. Climate*, **12**, 170-184.

Zhang, M. H., and coauthors, 2004: Comparing clouds and their seasonal variations in 10 atmospheric general circulation models with satellite measurements, to be submitted to Special Issue of ARMCPM, *J. Geophys. Res.*.

Zuidema, P., 1998: The 600−800-mb minimum in tropical cloudiness observed during TOGA COARE, *J. Atmos. Sci.*, **55**, 2220-2228.

Figure Captions

Fig. 1 Zonal-mean frequency distributions of total cloud amount (dotted), the 5-km overcast amount (solid), and the 5-km overcast amount with Pc < 500 mb (dashed) as functions of latitude obtained for April 2001.

Fig. 2 Zonal-mean frequency distributions of cloud amounts obtained for the five cloud categories of High1, High2, High3, Mid, and Low1. Results are plotted separately for each month and over ocean and land.

Fig. 3 Frequency distributions of Pc obtained for the six cloud categories of High1, High2, High3, Mid, Low1, and Low2. Results shown separately for each month and over ocean and land. Note that the frequencies of High1, Low1, and Mid are connected as one line and the total frequency of all clouds is plotted in thick solid lines.

Fig. 4 Same as in Fig. 3, except for the frequency distribution of t_{VIS}. Note that the frequencies of High3 and Mid clouds are added and plotted as one line.

Fig. 5 Frequencies of occurrence of the 5-km overcast Pc and t_{VIS} obtained from the four-month near-global dataset for a) the MODIS standard product and b) the overlapped retrievals. Results are shown separately for over ocean (left sub-panel) and over land (right sub-panel). The numbers in each sub-panel indicated the total percentages of Pc above (↑) and below (↓) 530 mb.

Fig. 6 Latitudinal distributions of the zonal-mean Pc (a), Tc (b), and t_{VIS} (c) obtained for the six cloud categories of High1, High2, High3, Mid, Low1, and Low2. Results are plotted separately for January, April, July, and October 2001.

Fig. 7 Geographic distributions of the total high-cloud (High1, High2 and High3) amount obtained for a) January, b) April, c) July, and d) October, 2001.

Fig. 8 Same as in Fig.7, except for the overlapped (High2/Low2) cloud amount.

Fig. 9 Same as in Fig.7, except for the Mid cloud amount.

Fig. 10 Same as in Fig.7, except for the total low-cloud (Low1 plus Low2) amount.

Fig. 11 Latitudinal distributions of zonal-mean t_{VIS} obtained from the MODIS standard products for April 2001. Note that High2* is from the MODIS single-layered retrieval, so there is no Low2.

Fig. 12 Comparisons of zonal-mean cirrus t_{VIS} inferred from 11-μm e_{hc} and from a) MODIS 0.86-μm reflectance for over ocean and b) MODIS 0.65-μm reflectance for over land. Results are obtained from January, April, July, and October 2001. Solid lines are the least squares fit.

Fig. 13 Latitudinal distributions of the zonal-mean e_{hc} obtained for High1, High2, and High3 cloud categories and for the High2* category from the MODIS standard product. Results are plotted for April 2001.

Table 1. Absolute and relative frequencies of occurrence of High1, High2, High3, Mid, and Low1 clouds obtained for each month of January, April, July and October 2001. Absolute frequencies (upper table) are computed as the percentage of occurrence out of all MODIS pixels and relative frequencies (lower table) are out of all 5-km overcast scenes. Results are given separately for ocean/land.

	Jan 2001	Apr 2001	Jul 2001	Oct 2001	Mean
Absolute (%)					
High1	4.3/ 5.5	4.6/ 4.8	3.4/ 3.7	4.0/ 5.2	4.1/ 4.8
High2	12.3/14.0	14.3/12.6	9.9/ 9.0	12.8/12.7	12.3/12.1
High3	7.6/ 9.3	7.9/ 7.6	7.2/ 7.6	7.9/ 9.1	7.6/ 8.4
Mid	2.3/ 1.4	1.2/ 1.0	1.8/ 2.2	1.5/ 1.1	1.7/ 1.4
Low1	22.4/13.6	18.8/14.0	20.4/16.2	20.6/14.5	20.6/14.6
Relative (%)					
High1	8.8/12.5	9.9/11.9	7.9/ 9.5	8.6/12.2	8.8/11.5
High2	25.2/32.0	30.5/31.5	23.3/23.4	27.2/29.8	26.6/29.2
High3	15.6/21.2	16.9/18.9	16.8/19.6	16.9/21.3	16.6/20.2
Mid	4.6/ 3.2	2.6/ 2.6	4.3/ 5.6	3.3/ 2.6	3.7/ 3.5
Low1	45.8/31.1	40.1/35.1	47.7/42.0	44.0/34.1	44.4/35.6

Table 2. Mean Pc, Tc, and t_{VIS} for High1, High2, High3, Mid, Low1, and Low2 cloud categories and mean e_{hc} for High1, High2 and High3. The means are given separately for ocean/land in each month. The overall mean of the four months is also given in last column.

	January 2001	April 2001	July 2001	October 2001	Mean
Pc (mb)					
High1	285/253	262/263	289/293	283/262	280/268
High2	322/292	307/300	322/324	320/302	318/304
High3	285/252	265/261	276/280	271/254	274/262
Mid	556/558	555/558	556/557	555/558	556/558
Low1	757/759	762/754	762/756	758/763	760/758
Low2	705/705	712/706	706/700	707/708	708/705
Tc (K)					
High1	229/225	226/226	233/234	230/228	230/228
High2	236/232	234/233	238/240	236/235	236/235
High3	229/224	226/225	230/231	227/226	228/227
Mid	264/267	264/265	267/268	264/266	265/267
Low1	278/280	278/278	280/281	278/280	279/280
Low2	276/277	276/276	278/278	276/278	277/277
t_{VIS}					
High1	1.45/1.38	1.35/1.39	1.51/1.57	1.40/1.41	1.43/1.44
High2	1.60/1.47	1.40/1.40	1.63/1.67	1.55/1.54	1.54/1.52
High3	21.1/21.2	22.4/19.0	23.1/22.3	22.6/21.4	22.3/21.0
Mid	15.9/13.8	16.5/14.8	17.5/17.0	17.9/15.2	17.0/15.2
Low1	10.8/10.1	10.7/10.6	10.4/10.8	11.1/10.6	10.8/10.5
Low2	13.3/12.2	14.3/12.6	13.8/13.9	14.0/13.4	13.8/13.0
e_{hc}					
High1	0.52/0.51	0.50/0.51	0.54/0.55	0.51/0.52	0.52/0.52
High2	0.54/0.51	0.49/0.49	0.55/0.56	0.53/0.53	0.53/0.52
High3	0.92/0.91	0.91/0.91	0.92/0.92	0.92/0.92	0.92/0.92

Table 3. Mean t_{VIS} for High1, High2*, High3, Mid, and Low1 and mean e_{hc} for High2* as obtained from the MODIS standard retrieval products. The High2* is assuming single-layer cloud with no presence of low cloud. The means are given in the format similar to those shown in Table 2.

	January 2001	April 2001	July 2001	October 2001	Mean
t_{VIS}					
High1	1.69/1.65	1.65/1.73	1.77/1.89	1.65/1.73	1.69/1.75
High2*	12.5/10.8	12.3/11.9	12.6/13.2	12.8/11.9	12.6/12.0
High3	25.9/24.8	25.4/24.5	27.1/27.4	26.9/25.3	26.3/25.5
Mid	16.1/13.5	16.8/15.4	17.1/16.5	18.0/15.0	17.0/15.1
Low1	11.2/10.5	11.0/11.1	10.8/11.4	11.3/10.9	11.1/11.0
e_{hc}					
High2*	0.64/0.61	0.61/0.60	0.64/0.65	0.64/0.62	0.63/0.62

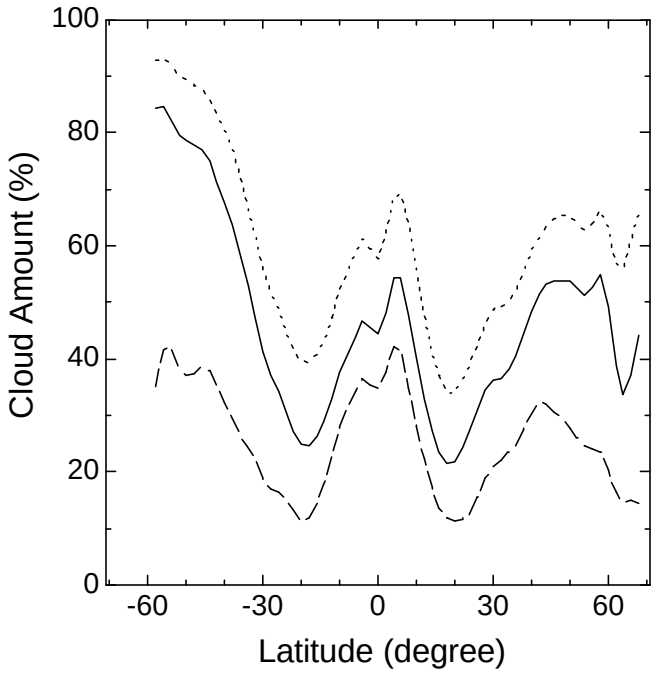

Fig. 1 Zonal-mean frequency distributions of total cloud amount (dotted), the 5-km overcast amount (solid), and the 5-km overcast amount with Pc < 500 mb (dashed) as functions of latitude obtained for April 2001.

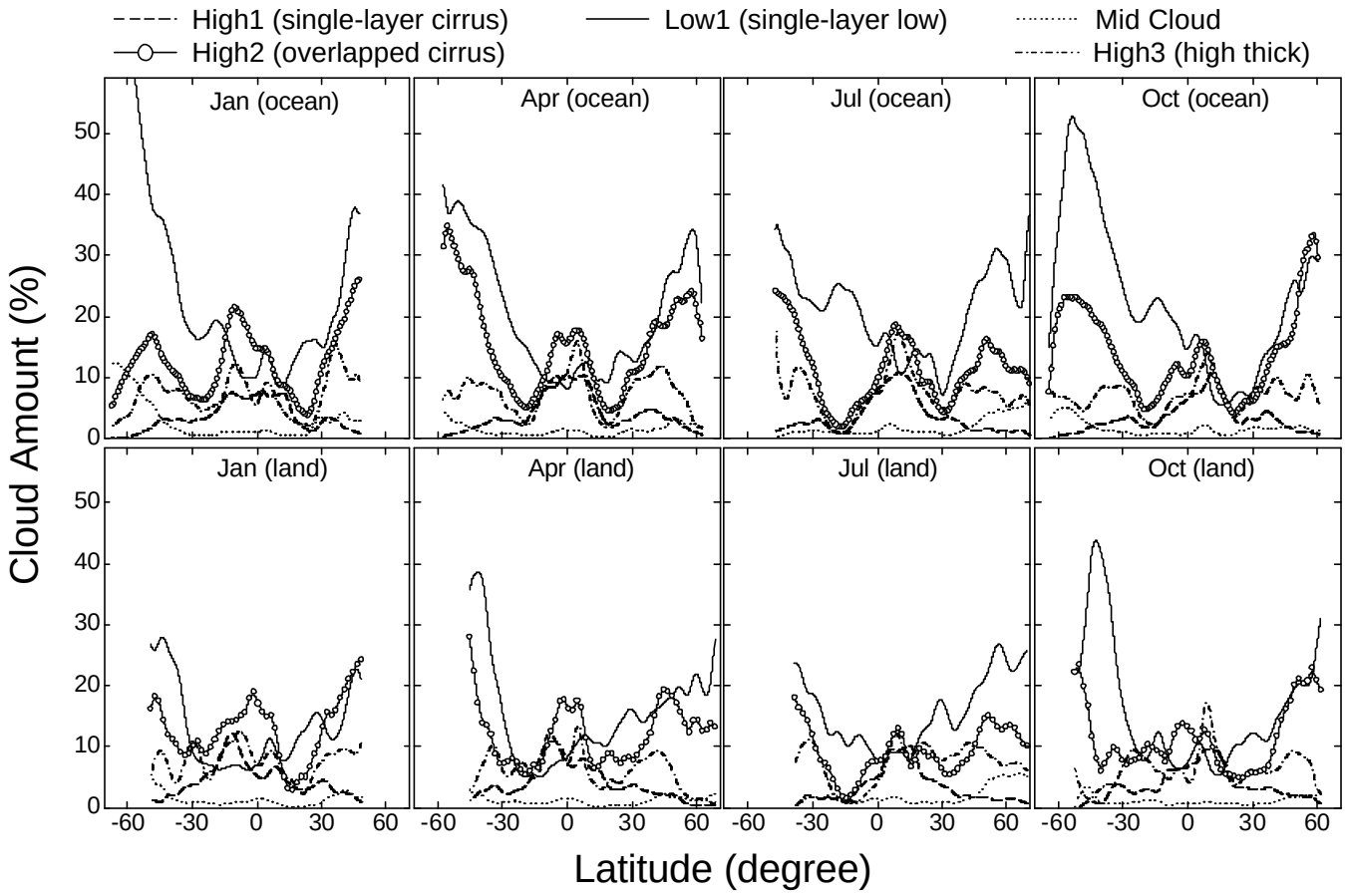

Fig. 2 Zonal-mean frequency distributions of cloud amounts obtained for five cloud categories of High1, High2, High3, Mid, and Low1. Results are plotted separately for each month and over ocean and land.

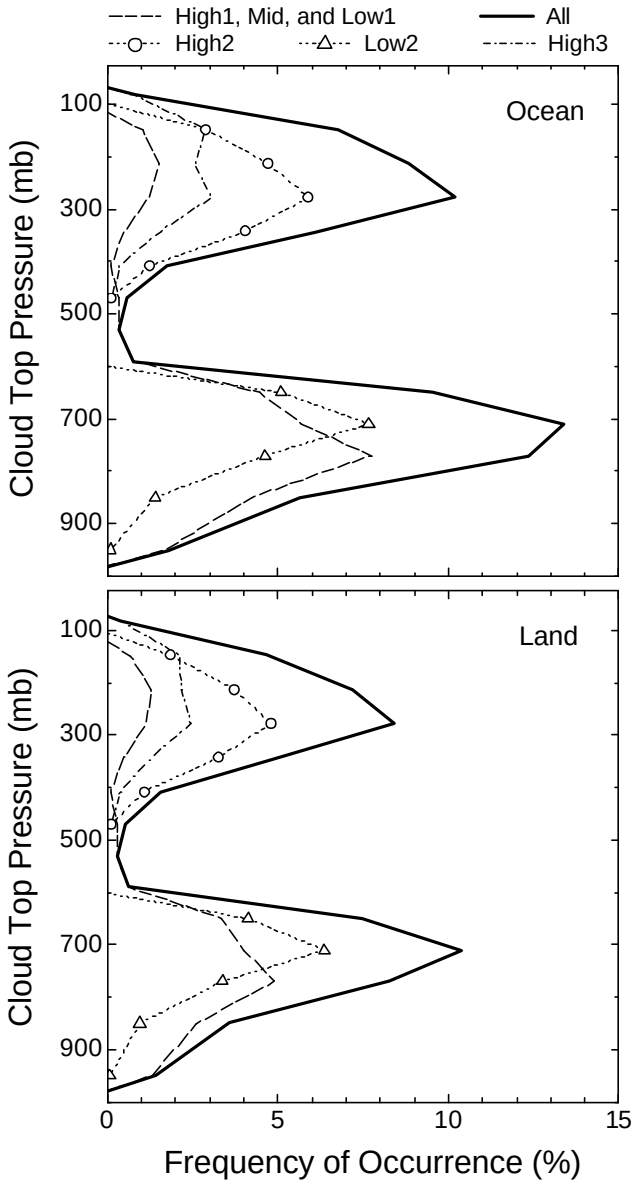

Fig. 3 Frequency distributions of Pc obtained for the six cloud categories of High1, High2, High3, Mid, Low1, and Low2. Results are obtained for April 2001 and shown separately for over ocean and over land. Note that the frequencies of High1, Low1, and Mid are connected as one line and the total frequency for all clouds is plotted in thick solid lines.

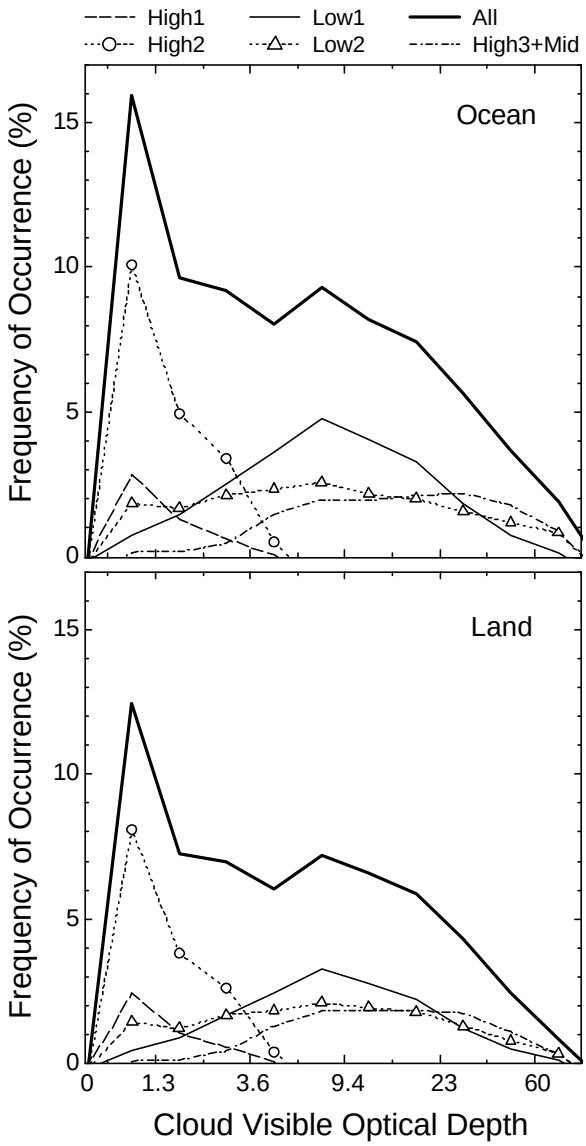

Fig. 4 Frequency distributions of t_{VIS} obtained for the six cloud categories of High1, High2, High3, Mid, Low1, and Low2. Results are obtained for April 2001 and shown separately for over ocean and over land. Note that the frequencies of High3 and Mid clouds are added and plotted as one line and the total frequency for all clouds is plotted in solid line.

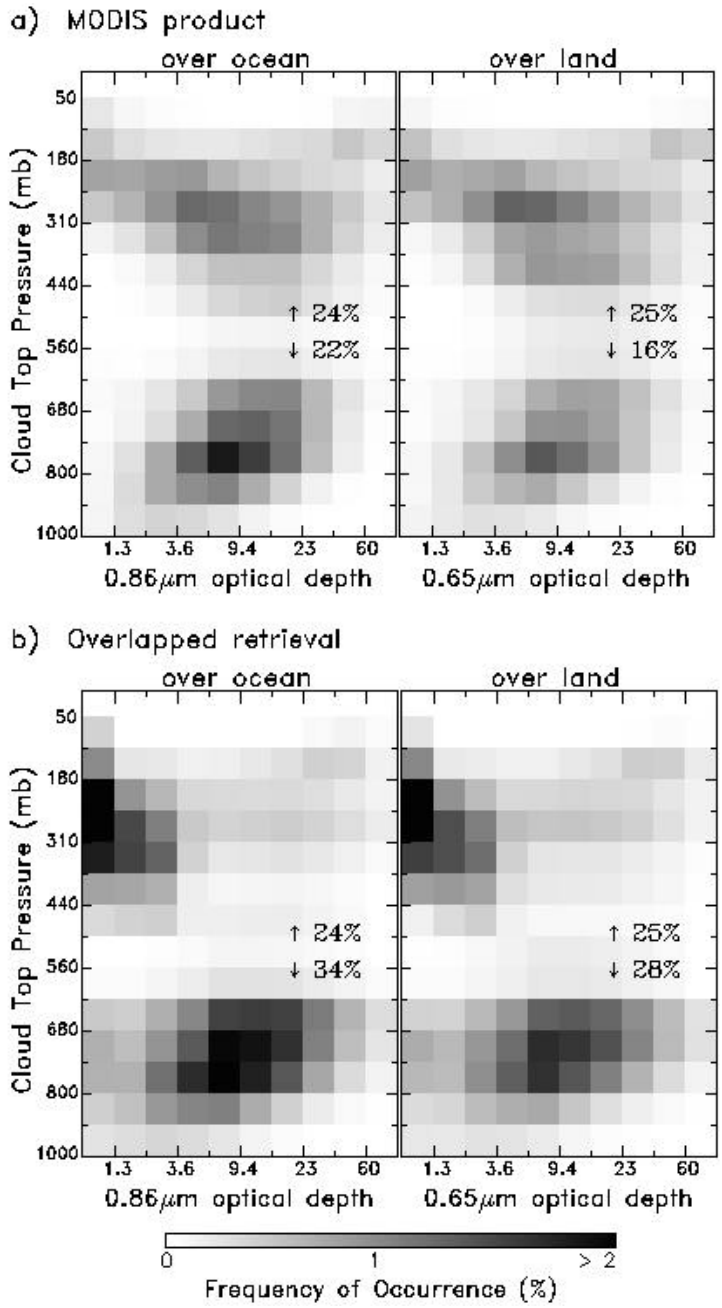

Fig. 5 Frequencies of occurrence of the 5-km overcast Pc and t_{VIS} obtained from the four-month near-global dataset for a) the MODIS standard product and b) the overlapped retrievals. Results are shown separately for over ocean (left sub-panel) and over land (right sub-panel). The numbers in each sub-panel indicated the total percentages of Pc above (↑) and below (↓) 530 mb.

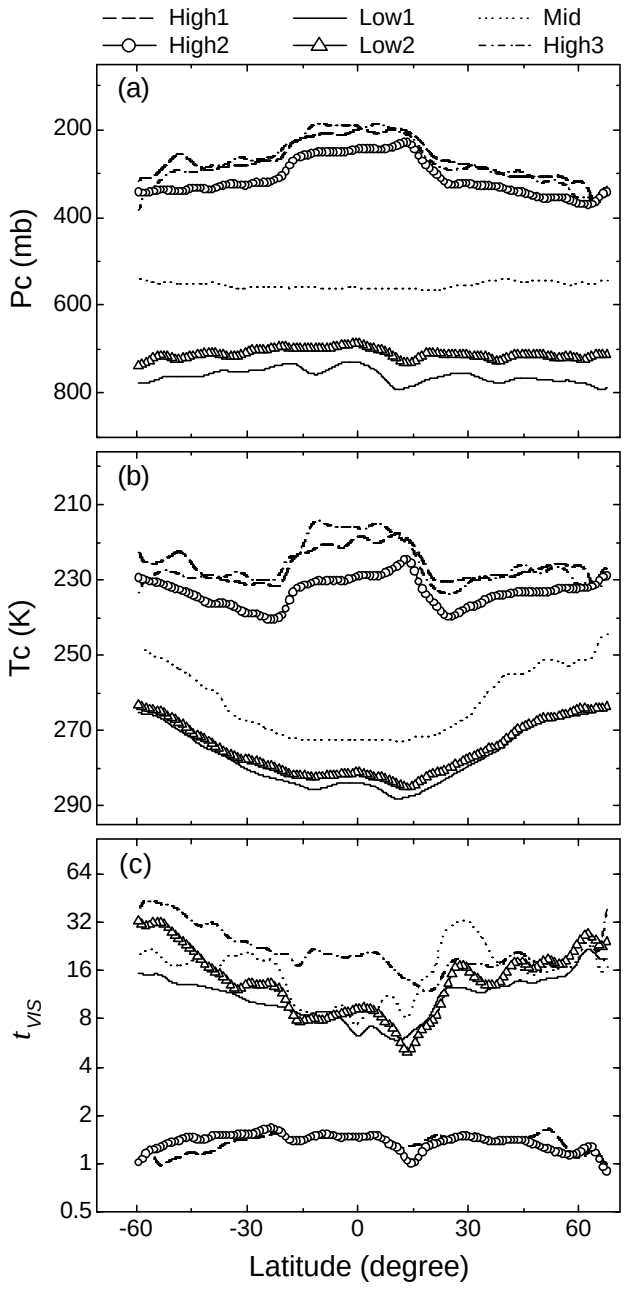

Fig. 6 Latitudinal distributions of the zonal-mean Pc (a), Tc (b), and t_{VIS} (c) obtained for the six cloud categories of High1, High2, High3, Mid, Low1, and Low2. Results show for April, 2001.

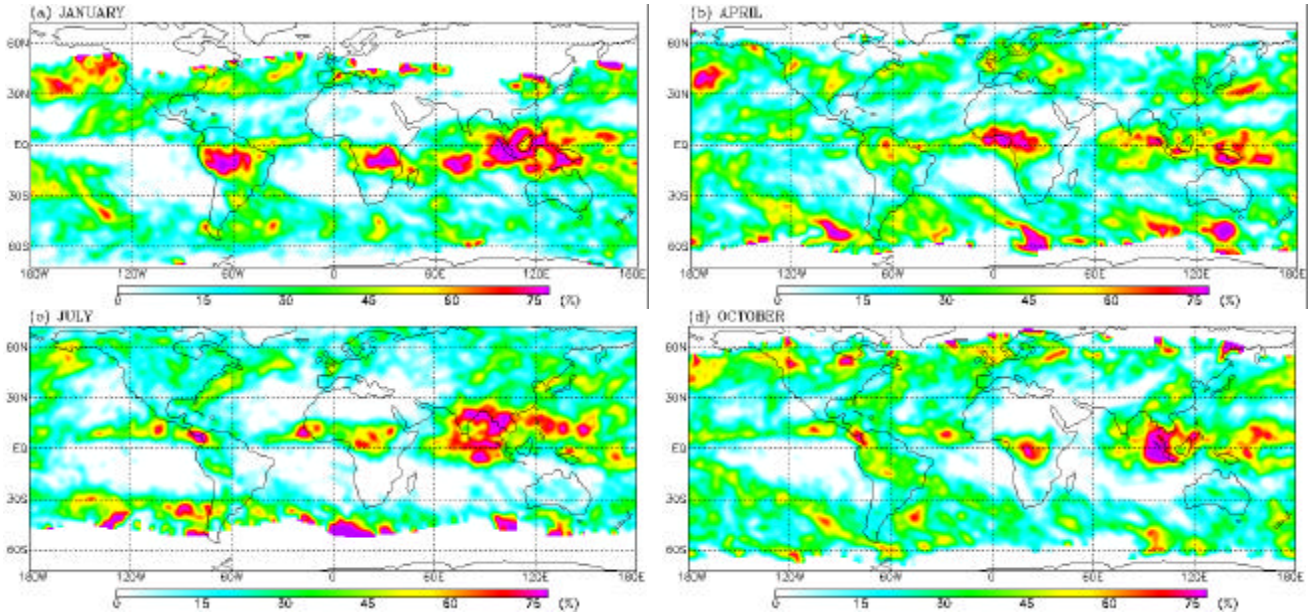

Fig. 7 Geographic distributions of the total high-cloud (High1, High2 and High3) amount obtained for a) January, b) April, c) July, and d) October, 2001.

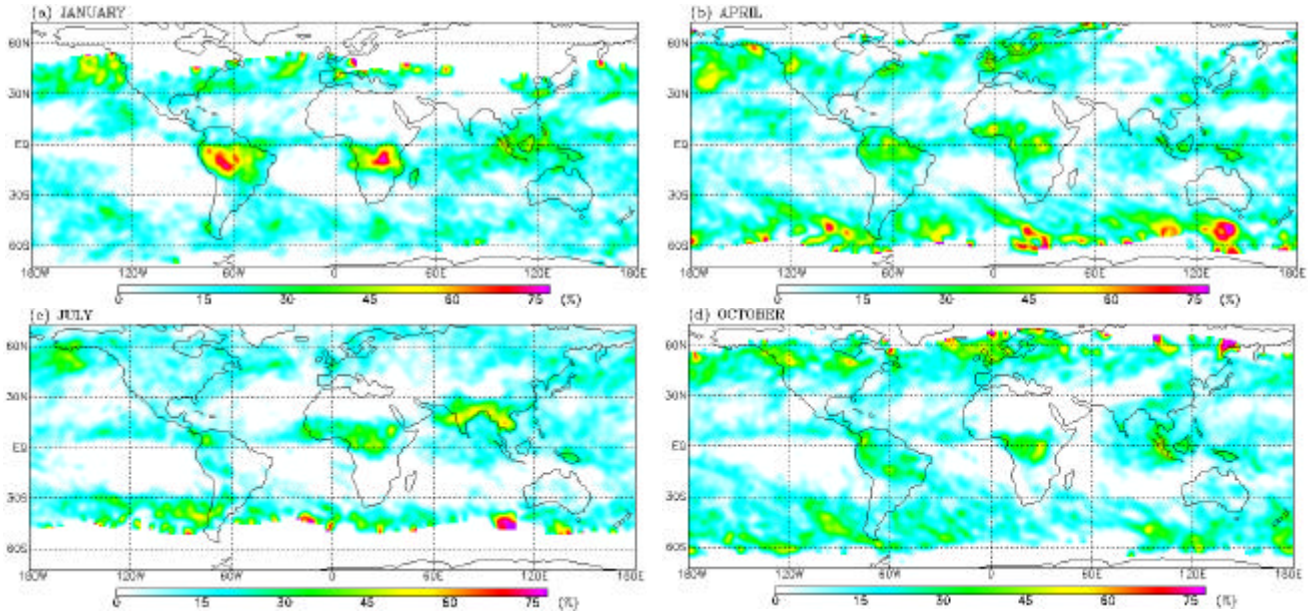

Fig. 8 Same as in Fig.7, except for the overlapped (High2/Low2) cloud amount.

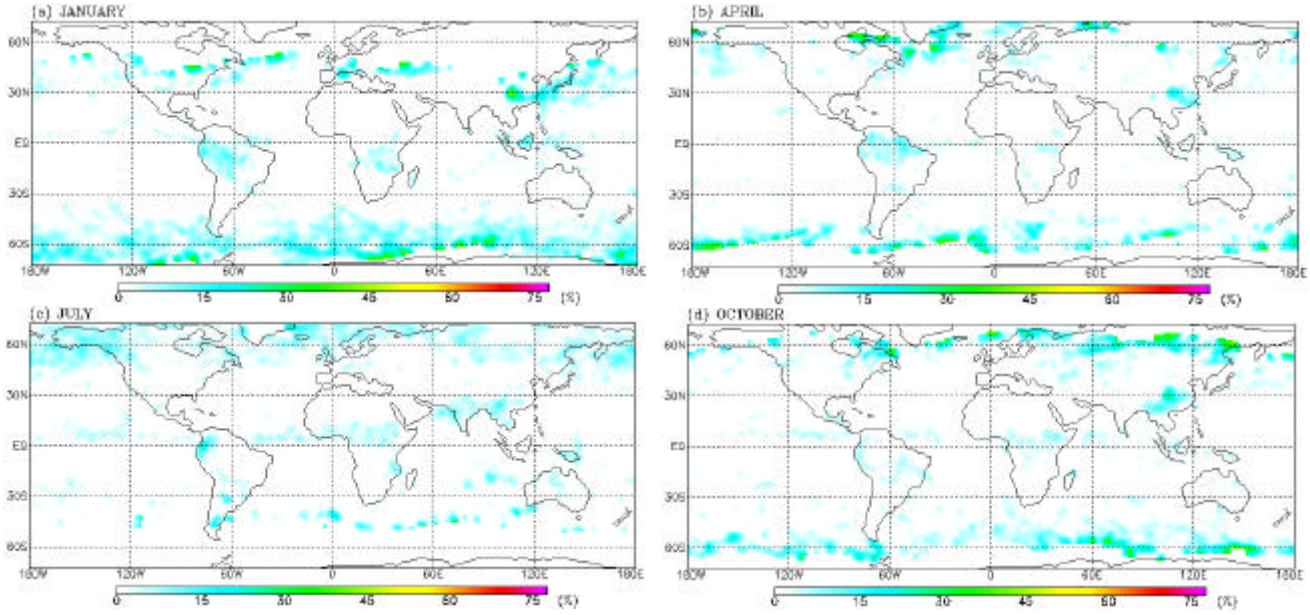

Fig. 9 Same as in Fig.7, except for the Mid cloud amount.

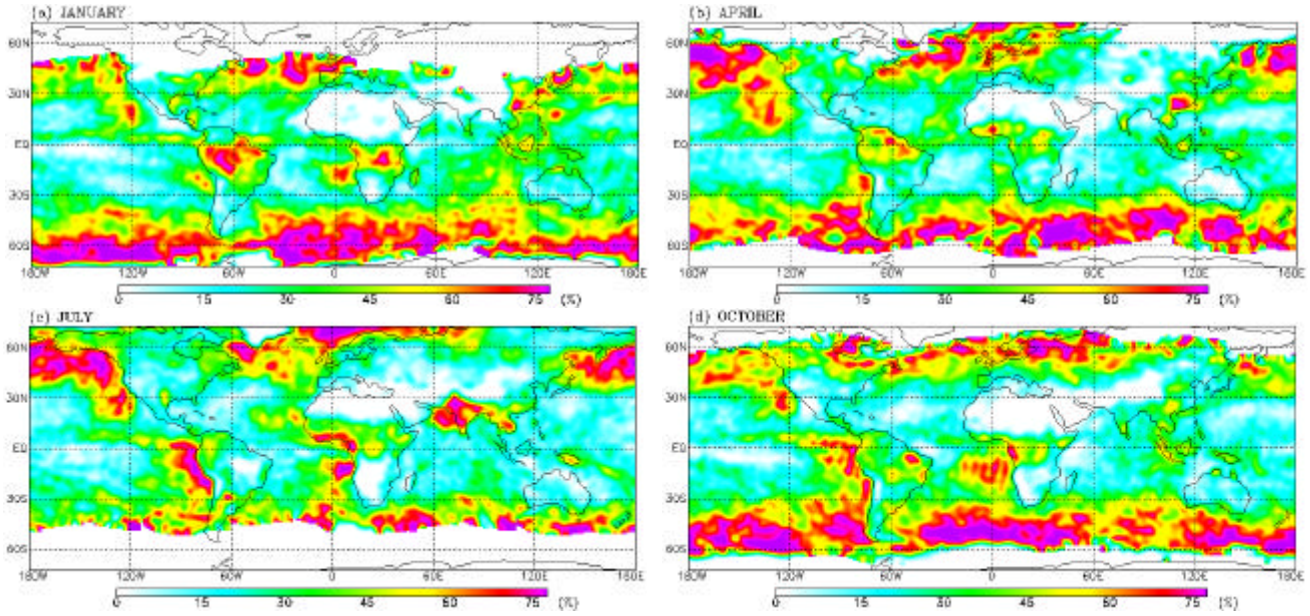

Fig. 10 Same as in Fig.7, except for the total low-cloud (Low1 plus Low2) amount.

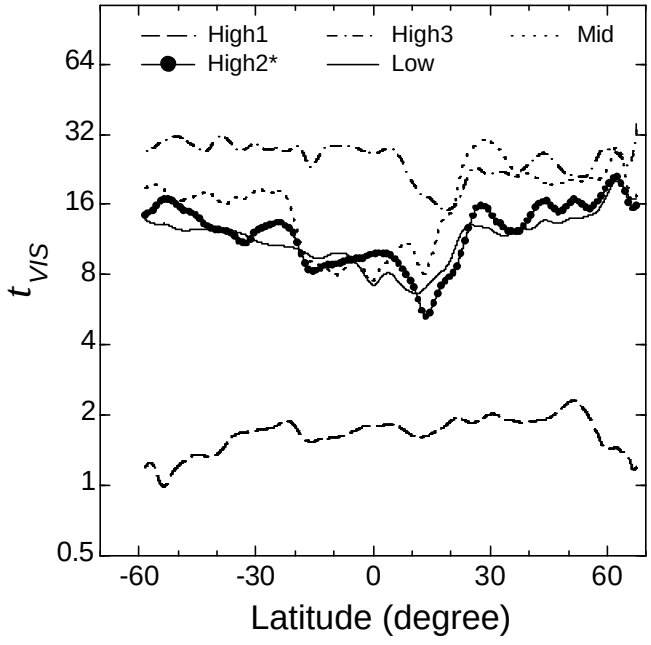

Fig. 11 Latitudinal distributions of zonal-mean t_{VIS} obtained from the MODIS standard products for April 2001. Note that High2* is from the MODIS single-layered retrieval, so there is no Low2.

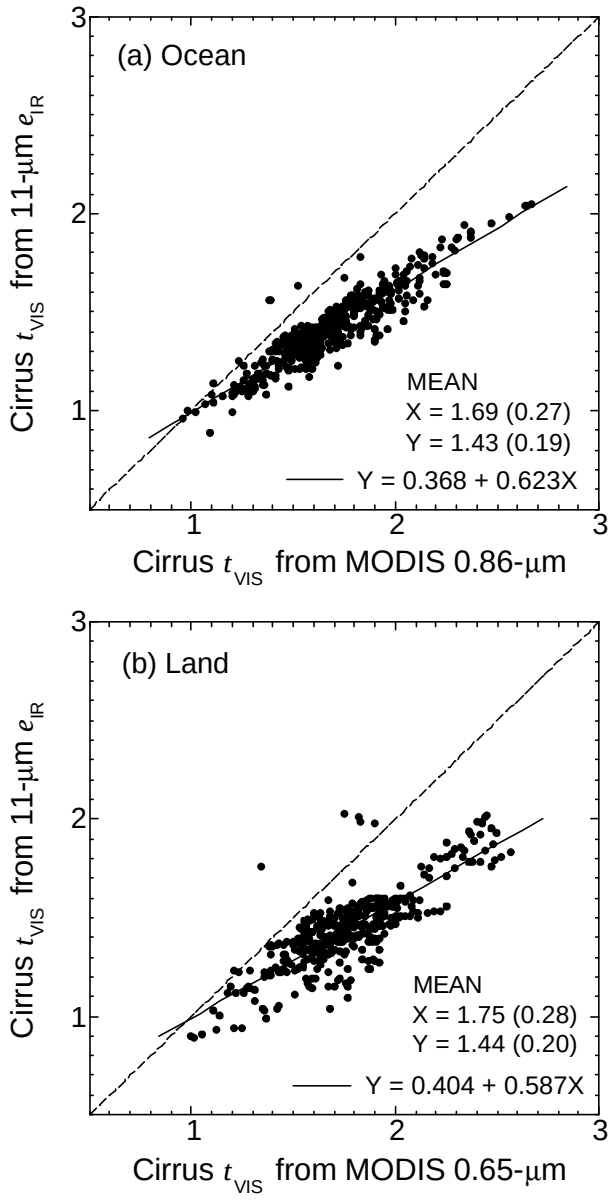

Fig. 12 Comparisons of zonal-mean cirrus t_{VIS} inferred from 11-μm e_{hc} and from a) MODIS 0.86-μm reflectance for over ocean and b) MODIS 0.65-μm for over land. Results are obtained from January, April, July, and October 2001. Solid lines are the least squares fit.

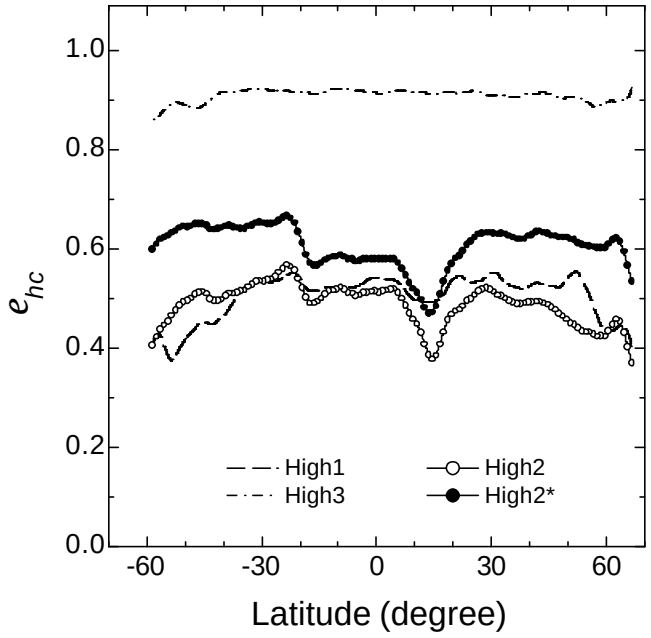

Fig. 13 Latitudinal distributions of the zonal-mean e_{hc} obtained for High1, High2, and High3 cloud categories and for High2* from the MODIS standard product. Results are plotted for April 2001.